Hindawi
Advances in Civil Engineering
Volume 2023, Article ID 7689445, 15 pages
https://doi.org/10.1155/2023/7689445

Research Article

Effect of SiO_2 Methyl Modification on the Performance of Nondispersible Underwater Concrete and Reinforcement Mechanism

Weiqiu Zhong, Longlong Zheng, Yongkang Shen, Wuxu Li, and Lingwei Zeng

School of Urban Planning and Municipal Engineering, Xi'an Polytechnic University, Xi'an 710600, China

Correspondence should be addressed to Weiqiu Zhong; zhongweiqiu@xpu.edu.cn

Received 10 March 2023; Revised 29 June 2023; Accepted 26 July 2023; Published 16 August 2023

Academic Editor: Robert Černý

The effect of SiO_2 methyl modification (CH_3-NS) on various properties of the nondispersible underwater concrete (UWC) was evaluated. The fluidity and antiwashout resistance of the UWC mixture were evaluated by various tests. Concrete specimens were designed in the two different damage states, i.e., P-type and Z-type. The compressive strength test, contact angle test, Fourier transform infrared spectroscopy (FTIR), and scanning electron microscopy (SEM) techniques were performed to analyze them. The experimental results showed that adding CH_3-NS increased the fluidity of the UWC. When too much CH_3-NS was added, the antiwashout resistance was reduced The CH_3-NS doping should not exceed 3.0%. For P-type specimens, adding uncalcined CH_3-NS improved the strength of the reinforced specimens compared to calcined CH_3-NS, the value was 17.9%. And the peak and ultimate stresses of the specimens were shifted forward by 18.1 and 4.8%, respectively. The polar force component magnitude of the surface tension of the specimen was the major factor affecting the surface free energy of P-type specimens. Different CH_3-NS statuses and the properties of specimens were the major factors affecting the surface free energy of Z-type specimens. Contact angle measurements, FTIR, and SEM showed that uncalcined CH_3-NS enhanced the hydrophobicity and reduced the surface free energy while increasing the density of UWC and thus enhancing its compressive strength.

1. Introduction

Recently, with the constant development of China's policy, coastal cities are increasing their investments in constructing hydroelectric buildings with great strategic importance, and the northwestern areas located inland are also beginning to build water conservancy projects [1, 2]. Meanwhile, countries around the world have gradually increased the construction of a large number of hydraulic structures, such as dams, hydropower stations, and reservoirs. Many countries are engaged in exploring and developing offshore gas and oil. As the performance of construction materials continues to improve, construction projects such as the coastal aquaculture, harbors, and marinas have also grown tremendously [3–5].

Due to long-term seawater scouring and erosive ions, many hydrotechnical constructions suffered different damage degrees. The existing strengthening methods are costly, traffic disrupting, and have a long construction time [6–11]. Therefore, several new reinforcement methods [12–14] have gradually emerged, relying on the performance of the nondispersible underwater concrete (UWC).

In the 1970s, UWC was first successfully placed underwater in the Federal Republic of Germany. In the following decades, countries worldwide introduced and improved UWC according to their needs. Existing research has discovered that adding low-surface free energy materials to UWC allows the water film to dry spontaneously, reducing the contact surface wettability. This can significantly lessen the impact of the water film on the reinforced surface, increasing the reinforcement effect [15]. At the same time, Courard et al. [16] found that the bond strength between reinforcement and concrete is directly related to the roughness of the concrete surface.

Many studies have been conducted on adding various admixtures to UWC to enhance its performance in recent years. Using 10 sets of UWC ratios, Wu et al. [17] concluded that the specimens mixed with silica fume were better at frost

Table 1: Properties of rapid hardening sulfoaluminate cement.

Specific surface area (m^2/kg)	Apparent density (kg/m^3)	Setting time (hr:min)		Compressive strength (MPa)		
495	3,020	Initial setting time	Final setting time	3d	7d	28d
		≥0:25	≤3:00	≥ 30.0	≥ 42.5	≥ 45.0

Table 2: Properties of fly ash.

Water content (%)	Specific surface area (m^2/kg)	Packing density (kg/m^3)	Density (g/cm^2)
5	5,000	1.001	2

Table 3: Properties of mineral powders.

Water content (%)	Specific surface area (m^2/kg)	Apparent density (kg/m^3)	Fineness (μm)
5	450	970	43

resistance than specimens mixed with fly ash, mineral powder, zeolite powder, and water repellent. Sikandar et al. [18] mentioned that gum Arabic, super absorbent, and Xanthan gum were the most suitable antiwashout admixtures (AWAs) for fabricating UWC. Wang et al. [19] reported that nanoparticles could significantly improve the compressive strength of UWC. As a result of the nanoparticles filling the voids in the concrete, its density increased. Researchers Liu et al. [20] found that adding mineral powder improved the pore size distribution and reduced the porosity of UWC, which improved the impermeability of concrete at a macrolevel. Jeon et al. [21] investigated the effect of nano-SiO_2 (NS) and MgO on the hydration characteristics and antiwashout resistance of UWC. In this study, they demonstrated that NS and MgO reduced slump flow, increased viscosity, and enhanced the antiwashout resistance of UWC. In the compressive strength test, NS increased the compressive strength of UWC, while MgO decreased the compressive strength.

NS is an amorphous material exhibiting high-pozzolanic activity, crystal nucleation, and microaggregate filling. NS has been shown to act as a crystal nucleus in cement, improving the material's mechanical properties and durability. However, the NS produced by the common sol–gel method tends to agglomerate easily. This is because it has more surfactants and greater surface energy and readily adsorbs water vapor from the environment. To a certain extent, this affects the application scope of NS. Through research on modification experiments, some scholars have demonstrated that methyltriethoxysilane (MTES) can be used to prepare SiO_2 methyl modification (CH_3-NS). Yang and Chen [22] found that the silica gel membrane's surface free energy and surface wettability decreased significantly with the ratio of MTES to tetraethyl orthosilicate. According to them, hydrogen bonds are primarily responsible for this effect. Using the sol–gel method, Yang et al. [23] produced Pd-doped CH_3-NS thin film materials. This experiment demonstrated that dimethylformamide did not significantly affect the chemical structure of Pd-doped SiO_2 thin film materials. Nevertheless, it delayed the oxidation of metallic palladium to palladium oxide in the air.

Overall, reviewing the literature, the research on UWC has made some progress, and many scholars are looking for better admixtures to improve the performance of UWC. Nevertheless, this research is still underway. Although the performance of SiO_2 has been studied, there is little work available on CH_3-NS. CH_3-NS is a novel material that is attractive. Currently, it is mostly utilized in engineering to increase the mechanical properties of concrete, the performance of recycled concrete, and to produce waterproof coatings. Due to its remarkable qualities, it can also be used to address the existing hydrotechnical construction issues. Therefore, the prime aim of this work is to research the advantages of CH_3-NS in fabricating UWC and reinforcement applications. This study prepared CH_3-NS as a mineral admixture for fast-setting UWC. Meanwhile, this study investigated its effect on the fluidity, antiwashout resistance, compression strength, and reinforcement properties of UWC. In addition, this study considered contact angle tests, Fourier transform infrared spectroscopy (FTIR), and scanning electron microscopy (SEM) to investigate the mechanism.

2. Materials and Methods

2.1. Materials. About 42.5 grade rapid hardening sulphoaluminate cement obtained from a company (China, Shandong) was used as the primary binding material. Its physical properties are shown in Table 1. Adding fly ash and mineral powder can reduce the amount of cement and aggregates [24–26]. Zhang and Dong [27] discovered that fly ash improved the concrete fluidity and increased the underwater/in-air strength ratio of UWC. Furthermore, it allowed for even distribution of the material's pore size. Zhang et al. [28] incorporated both fly ash and mineral powder into UWC. He found that when only one material is added, the flow of the concrete is reduced, but the strength is increased. Class I fly ash and S95 mineral powder from a company (China, Henan), were used in this study. Its physical properties are shown in Tables 2 and 3. Specifically, the diameter of the coarse aggregate was from 5 to 20 mm and had a good gradation; fine aggregates with a fineness modulus of 2.5,

Table 4: Physical parameters of the precursors.

Medicine	Molecular formula	Molecular weight	Boiling point
TEOS	$C_8H_{20}O_4Si$	208.327	165.5°C
MTES	$C_7H_{18}O_3Si$	178.302	142°C

Figure 1: The preparation process of CH_3-NS.

medium sand. This test utilized two admixtures, UWB-II AWA, and a super plasticizer. The UWB-II AWA was provided by an institute in Tianjin, China.

2.2. Preparation of CH_3-NS. Yang et al. [29] used TEOS and MTES as base materials and dilute nitric acid (HNO_3) as a catalyst. In a certain molar ratio, CH_3-NS was successfully prepared.

First, precursors were selected. The TEOS and MTES used in this experiment were both from the same company (China, Shanghai). Their parameters are shown in Table 4.

Second, TEOS, MTES, EtOH, H_2O, and HNO_3 were weighed according to the mass ratio of 1/0.8/7.6/7.2/0.085 and placed into each cup. At the same time, the first three precursors were sequentially added to the triplex container. When they were completely mixed, they were put into the ice–water mixture. The prepared homogeneous solution was placed in a magnetic stirrer, and a mixture of water and dilute nitric acid was added dropwise. Then, under stirring reflux at 60°C, CH_3-NS sol was obtained by cooling. First, the CH_3-NS sol was placed in a Petri dish and then dried in an oven for 12 hr. After that, it was coarsely ground in a ceramic container and finely ground in an agate container. Then, the uncalcined CH_3-NS sol was obtained. The calcined CH_3-NS was prepared by calcination in a muffle furnace for 6 hr at 350°C. Finally, this study prepared CH_3-NS that could be incorporated into UWC as an admixture by further coarse and fine grinding of CH_3-NS. The preparation process is shown in Figure 1.

2.3. Mix Proportions and Fabrication of Specimens. In this study, UWC was prepared according to the strength grade of

Table 5: Concrete mix design (kg/m^3).

Cement	Fly ash	Mineral powders	Fine aggregate	Coarse aggregate	Water	UWB-II AWA	Super plasticizer	CH_3-NS(%)
333.4	71.4	71.4	689.5	1034.3	200	11.9	4.8	1
333.4	71.4	71.4	689.5	1034.3	200	11.9	4.8	3
333.4	71.4	71.4	689.5	1034.3	200	11.9	4.8	5
333.4	71.4	71.4	689.5	1034.3	200	11.9	4.8	7
333.4	71.4	71.4	689.5	1034.3	200	11.9	4.8	9

Table 6: Performance requirements of UWC.

Experimental projects	Specific projects	Parameter requirements
Fluidity	Slump (mm)	230 ± 20
	Slump flow (mm)	450 ± 20
Antiwashout resistance	Loss of cement (g)	<1.5
	Suspended matter content (mg/L)	<150
	pH	<12
Underwater/in-air strength ratio (MPa)	7d	>35
	28d	>50

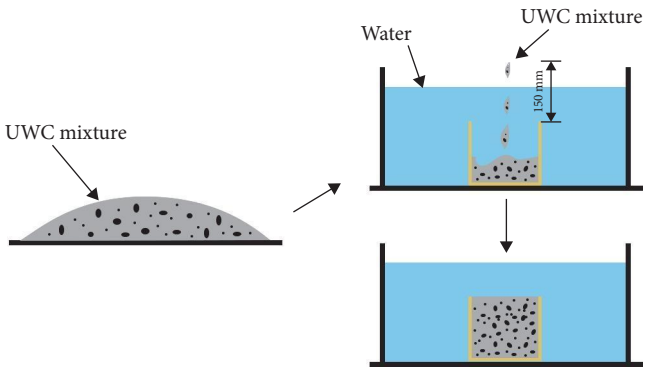

Figure 2: The UWC production process.

C30. Based on the specification (Q/CNPC 92-2003), a water/cement ratio of 0.42 was used [30]. CH_3-NS was selected for incorporation into UWC due to its excellent properties. Despite this, few studies have been conducted regarding the effect of its dosing on the performance of UWC. As a result, five groups of doping levels of 1%, 3%, 5%, 7%, and 9% were chosen to investigate the effect of CH_3-NS doping on UWC performance. The specific proportion of the mixture design is shown in Table 5.

The UWC specimens were prepared following the DL/T 5117-2021 [31]. The size of specimens is $150 \times 150 \times 150$ mm. The specific performance requirements are shown in Table 6. The process is shown in Figure 2.

2.4. Experiment Methods. As specified in DL/T 5117-2021, the concrete fluidity test consists primarily of the slump test and the slump flow test. The tests were carried out in accordance with the steps required by the specification, and the results were recorded.

This study used suspended matter content, pH, and turbidity measurement tests to measure the antiwashout resistance of the UWC mixes. The test water samples were made according to the method in the specification. The suspended solids content of the water samples were calculated using the weighing method. Using a pH meter, its pH was measured. The instrument used was a PHS-3C pH meter. The same water sample was used to measure turbidity in the turbidity machine. The instrument used was the SGZ-2 turbidity meter.

The cube compressive strength test was carried out by following the relevant provisions of DL/T 5117-2021, and each reported result was the average value for three test cubes. The UWC reinforcement test was conducted using concrete specimens in two different damage states. The first type of specimen used for running the UWC reinforcement test was a crushed concrete specimen. The specimen lost its corresponding load-carrying capacity. This is done to simulate severe natural disasters or human damage to the concrete. Two types of specimens were prepared, one with calcined CH_3-NS and the other with uncalcined CH_3-NS. They were numbered P-1 and P-2. Meanwhile, the reinforcement state was also divided into underwater and in-air. The artificially chiseled specimen is the second damaged condition of the concrete specimen. The depth of the cut is 3–4 cm. This is to simulate concrete with minor human damage. They have the same state as the first type. They were numbered Z-1 and Z-2. Table 7 and Figure 3 explain the meaning of the number of damaged specimens.

In this study, the impact of CH_3-NS on UWC reinforcement was analyzed by conducting the contact angle tests, FTIR, and SEM for examining hydration products and the microscopic morphology of damaged specimens.

3. Results and Discussion

3.1. Fluidity Test. Table 8 shows the material's fluidity after adding different doses of CH_3-NS. Figure 4(a) and 4(b) show

Table 7: Meaning of damaged specimen number.

Damaged specimen number	Meaning of number
P-1	Type I specimens mixed with uncalcined CH_3-NS
P-2	Type I specimens mixed with calcined CH_3-NS
Z-1	Type II specimens mixed with uncalcined CH_3-NS
Z-2	Type II specimens mixed with calcined CH_3-NS

(a) (b)

Figure 3: Concrete specimens of two different damage states: (a) crushed specimens and (b) chiseled specimens.

Table 8: The fluidity of the material after adding different doses of CH_3-NS.

Dosage of CH_3-NS (%)	Slump (mm)	Slump flow (mm)
1	225	440
3	235	458
5	240	472
7	250	475
9	230	465

the material's slump and slump flow after adding different doses of CH_3-NS.

Figure 4(a) shows the relationship between the slump of UWC and CH_3-NS dosing. The maximum slump value was obtained at a CH_3-NS admixture of 7%. The value was 250 mm. The minimum slump value was obtained at a CH_3-NS admixture of 1%. The value was 225 mm. This suggests that adding CH_3-NS influenced the slump of UWC.

Figure 4(b) shows that the slump flow and slump followed approximately the same trend. They both had maximum values at CH_3-NS of 7%. When CH_3-NS was 9%, they decreased sharply.

In conclusion, the addition of CH_3-NS improved the fluidity of the material. This is mainly because CH_3-NS is a spherical particle, which plays a ball effect in the concrete mixture. Furthermore, the data showed an abnormal decrease after increasing the CH_3-NS to 7%. Therefore, the CH_3-NS doping should not exceed 7.0% in accordance with Table 6.

3.2. Antiwashout Resistance. Table 9 shows the material's antiwashout resistance after adding different doses of CH_3-NS. Figure 5(a) and 5(b) show each water sample's suspended matter content and pH.

With an increase in CH_3-NS, the suspended matter content of the water sample increased. When CH_3-NS was dosed at 9%, the highest suspended matter content in the water sample was achieved, with a value of 195 mg/L. Meanwhile, with an increase in CH_3-NS, the pH of the water sample also increased. When CH_3-NS was dosed at 9%, the highest pH of the water sample was achieved, with a value of 12.35. Figure 5(c) shows the turbidity value of each water sample. According to this figure, all the water samples showed similar tendencies regarding the suspended matter content and turbidity values. The turbidity value of the water sample increased with an increase in CH_3-NS. When CH_3-NS was dosed at 9%, the highest turbidity value of the water sample was achieved, with a value of 430.5 NTU.

In summary, some of the data from the three types of tests seriously exceeded the requirements of Table 6. The primary cause of this is the precipitation of CH_3-NS and other substances while the UWC mix was in the water. Therefore, the CH_3-NS doping should not exceed 3.0% in accordance with Table 6.

3.3. Reinforcement Test

3.3.1. Compressive Strength Test for Standard Test Cube. Table 10 and Figure 6(a)–6(d) show compressive strength data for various doses of CH_3-NS and concrete ages.

A comparative analysis of the above data showed that the strength of concrete decreased slowly with increasing CH_3-NS admixture at 1%–3%. Comparing each dose level showed that UWC at 1% had the highest strength. This demonstrates that a large proportion of CH_3-NS did not improve concrete

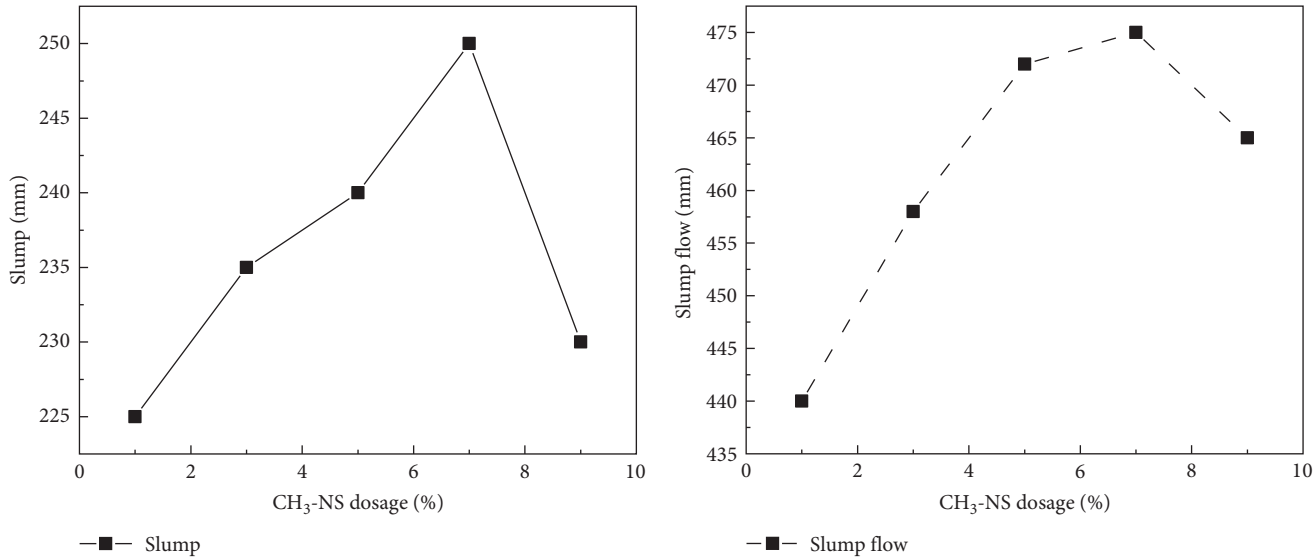

Figure 4: The fluidity of the material after adding different doses of CH_3-NS: (a) slump and (b) slump flow.

Table 9: The antiwashout resistance of the material after adding different doses of CH_3-NS.

Dosage of CH_3-NS (%)	Suspended matter content (mg/L)	Turbidity (NTU)	pH
1	142	336.7	11.65
3	168	377.2	11.89
5	185	410.5	12.08
7	190	425.6	12.2
9	195	430.5	12.35

strength in the subsequent admixture. Therefore, it is necessary to carry out further research.

In summary, the CH_3-NS doping should not exceed 3.0%.

3.3.2. After Reinforcement. Table 11 and Figure 7(a)–7(d) show the test results for each group of reinforcement concrete specimens.

Table 11, Figures 7(a), and 7(b) show that adding CH_3-NS of two different states affected the reinforcement performance of the P-type reinforcement concrete specimens; particularly, P-type reinforcement concrete specimens under the underwater conservation conditions. Compared to calcined CH_3-NS, uncalcined CH_3-NS increased its strength by 17.9%. Furthermore, these specimens exhibited a forward shift in peak and ultimate strains. The values were 18.1% and 4.8%, respectively. The state of CH_3-NS incorporation did not have a significant effect on the strength of P-type reinforcement concrete specimens under the in-air conservation conditions. From results, it is ascertained that the use of uncalcined CH_3-NS in P-type reinforcement concrete specimens under the underwater conservation may lead to producing a large number of tiny particles in the concrete microstructure, which may lead to densifying the microstructure. Therefore, incorporating uncalcined CH_3-NS was effective in enhancing the strength of P-type reinforcement concrete specimens under the underwater conservation conditions.

Table 11, Figures 7(c), and 7(d) demonstrate that adding different states of CH_3-NS did not significantly improve the strength of Z-type reinforcement concrete specimens. In addition, there was also no forward shift in peak and ultimate strains. This was due to the reinforcement concrete specimen itself. Because Z-type specimens were damaged concrete specimens after manual chiseling, they still possessed some load-bearing capacity, so the addition of CH_3-NS did not have a significant effect. In the later stages of the compressive strength test, the concrete on the reinforced side was also the first to be crushed. This further suggests that the original concrete provided the majority of the load-bearing capacity in the latter part of the test.

3.4. Contact Angle Test and Calculation of Surface Free Energy. In the contact angle test, the experimental samples were taken from the contact surface of the reinforced part of the specimens. Two polar–nonpolar liquid combinations were selected for this contact angle test; distilled water–diiodomethane and glycerin–diiodomethane. This test can determine the specimen's hydrophobicity. In this study, the contact angle sizes of the various reinforcement specimens were measured and used to calculate their surface free energy. The test images of partial contact angles are shown in Figure 8. By doing so, this study

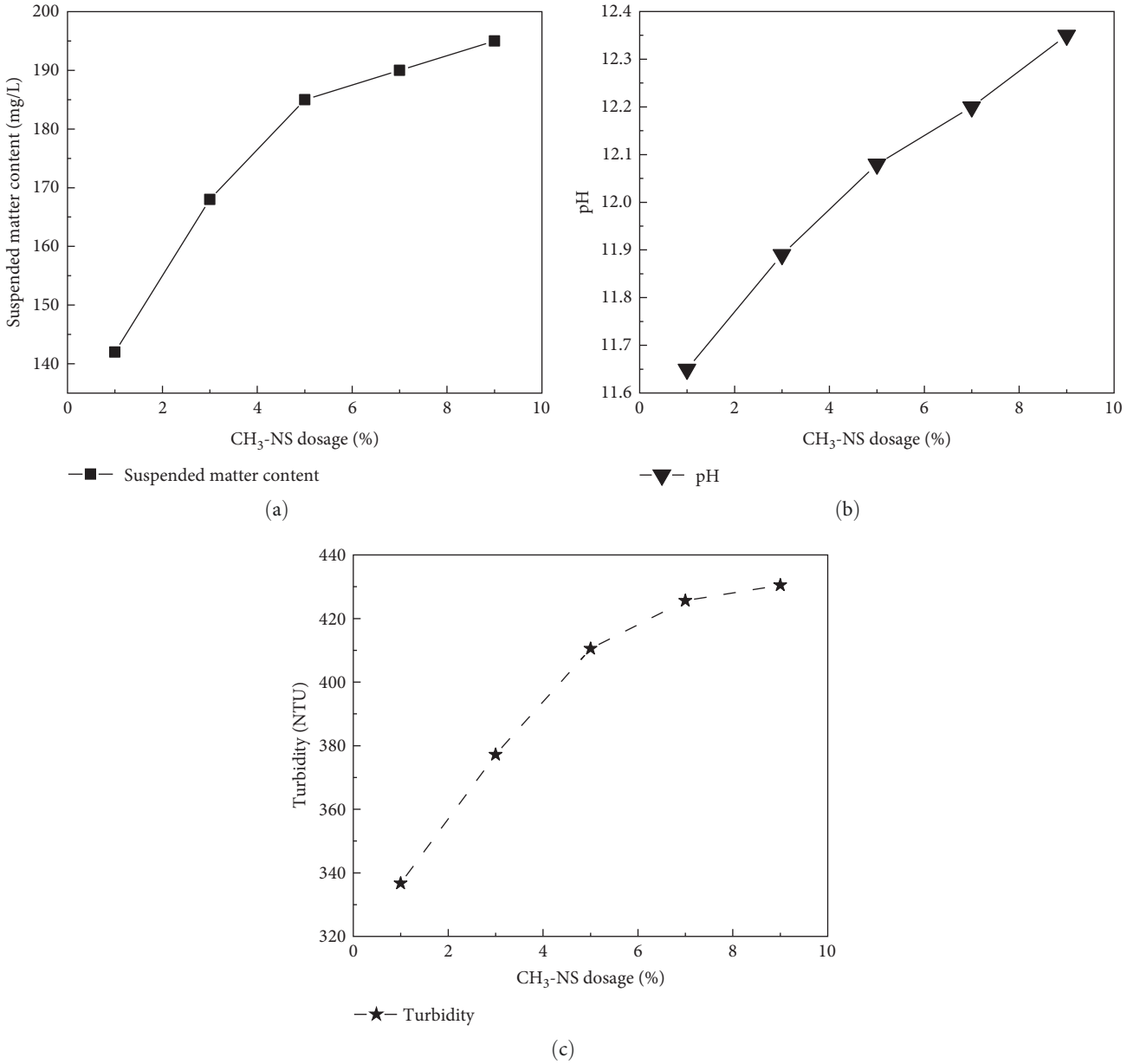

Figure 5: The antiwashout resistance of the material after adding different doses of CH_3-NS: (a) suspended matter content, (b) pH, and (c) turbidity.

Table 10: Compressive strength data for various doses of CH_3-NS and concrete ages (MPa).

Dosage of CH_3-NS (%)	1d Compressive strength		3d Compressive strength		7d Compressive strength		28d Compressive strength	
	In-air	Underwater	In-air	Underwater	In-air	Underwater	In-air	Underwater
1	24.5	17.8	25.6	19.9	45.2	34.5	56.9	45.2
3	15.0	12.0	20.1	15.6	42.0	33.2	49.8	40.2
5	19.4	14.5	21.6	16.5	40.8	32.0	52.6	43.8
7	20.1	16.8	24.2	17.8	41.6	35.0	54.8	45.8
9	23.1	17.6	27.8	20.0	43.9	36.9	57.0	47.6

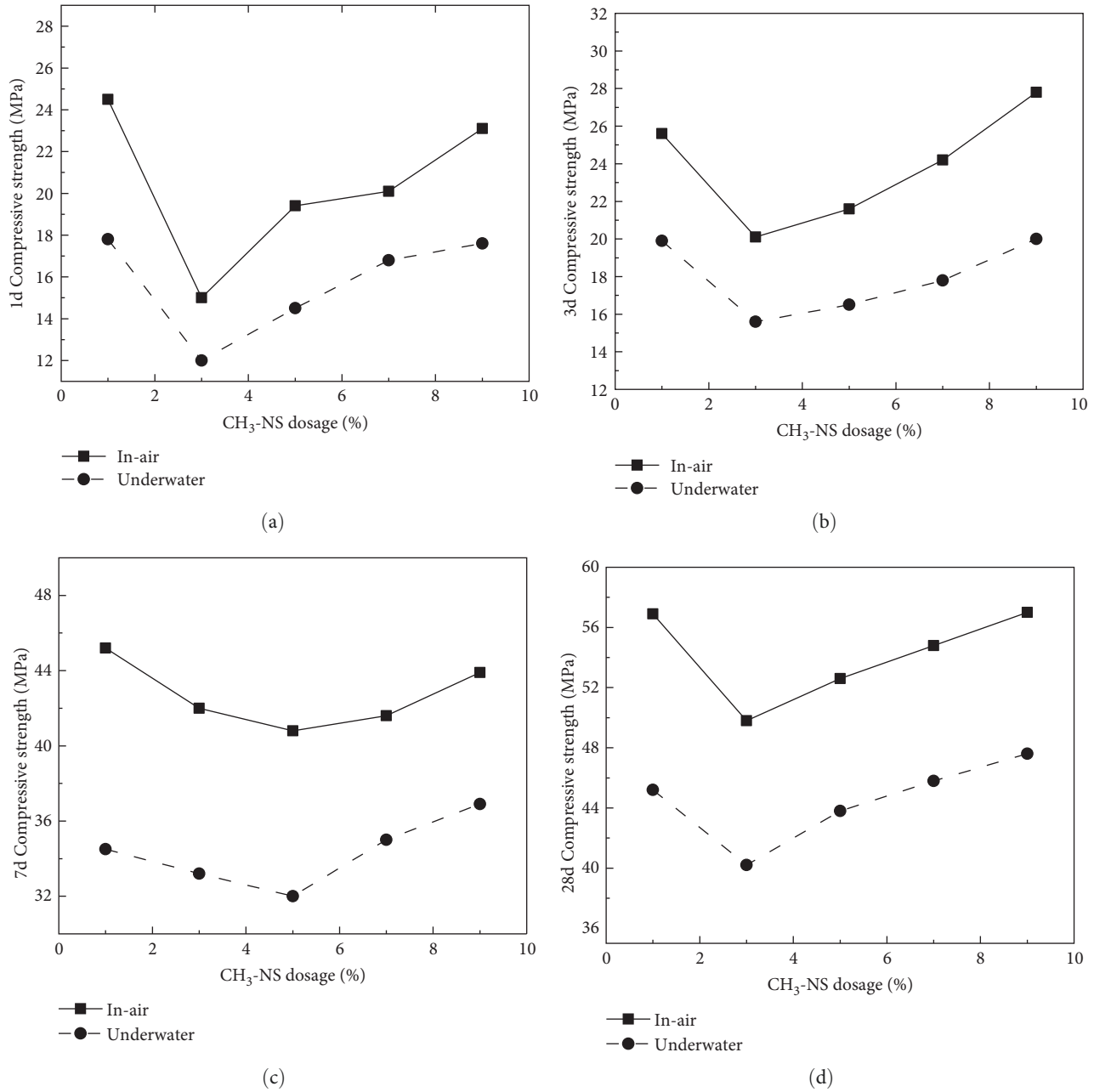

Figure 6: Compressive strength data for various doses of CH_3-NS and concrete ages: (a) 1d compressive strength, (b) 3d compressive strength, (c) 7d compressive strength, and (d) 28d compressive strength.

Table 11: Test data of reinforced specimens.

Category	Collapse load (kN)	Peak stress (MPa)	Peak strain	Ultimate strain
P-1(in-air)	766.85	34.08	4.81	5.35
P-1(underwater)	599.72	26.65	4.02	5.57
P-2(in-air)	730.31	32.46	3.92	5.41
P-2(underwater)	508.32	22.60	4.91	5.85
Z-1(in-air)	887.43	39.44	3.37	4.34
Z-1(underwater)	807.12	35.87	3.35	4.28
Z-2(in-air)	893.03	39.69	3.36	4.64
Z-2(underwater)	747.90	33.24	3.03	4.79

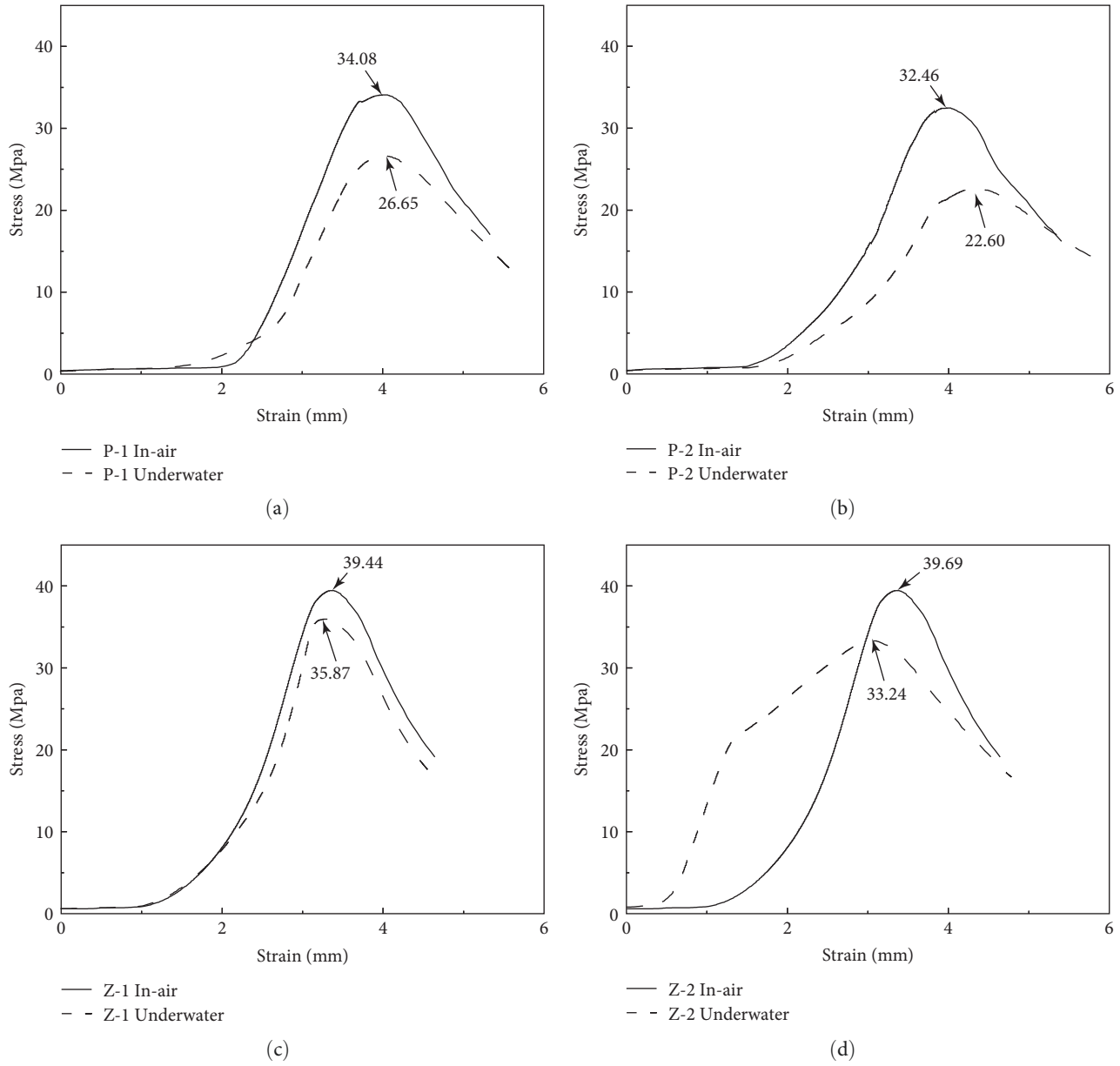

Figure 7: (a) The stress–strain curve of the P-1 specimens, (b) the stress–strain curve of the P-2 specimens, (c) the stress–strain curve of the Z-1 specimens, and (d) the stress–strain curve of the Z-2 specimens.

Table 12: Data of contact angle tests.

Category	Average value of contact angle (°)		
	Distilled water	Glycerin	Diiodomethane
P-1(in-air)	79.6	65.5	56.6
P-2(underwater)	73.9	62.7	53.4
Z-1(in-air)	57.3	51.8	46.5
Z-2(underwater)	57.3	51.2	42.1

gained a deeper understanding of the influence of CH_3-NS doping on the reinforcement specimen properties.

According to Table 12, the contact angle variation for the P-type specimens was relatively consistent for the polar liquids tests (distilled water and glycerin). In both, P-1 (in-air) was greater than P-1 (underwater), with 7.16% and 4.27% declines. Hence, the specimens' hydrophobic properties were relatively stable. In the same test, there was no

Table 13: Surface free energy and components of test water samples ($\times 10^{-5}$ N cm^{-1}).

Category	Water–diiodomethane			Glycerin–diiodomethane			Average surface free energy			
	γ_S^d	γ_S^P	γ_S	γ_S^d	γ_S^P	γ_S	γ_S^d	γ_S^P	γ_S	γ_S^P/γ_S
P-1 (in-air)	25.39	7.53	32.92	26.14	7.29	33.43	25.77	7.41	33.18	0.22
P-2 (underwater)	26.09	10.17	36.26	26.74	8.41	35.15	26.42	9.29	35.71	0.26
Z-1 (in-air)	26.56	20.21	46.77	27.89	15.36	43.25	27.23	17.79	45.01	0.40
Z-2 (underwater)	29.29	18.78	48.07	31.50	11.62	43.12	30.40	15.20	45.60	0.33

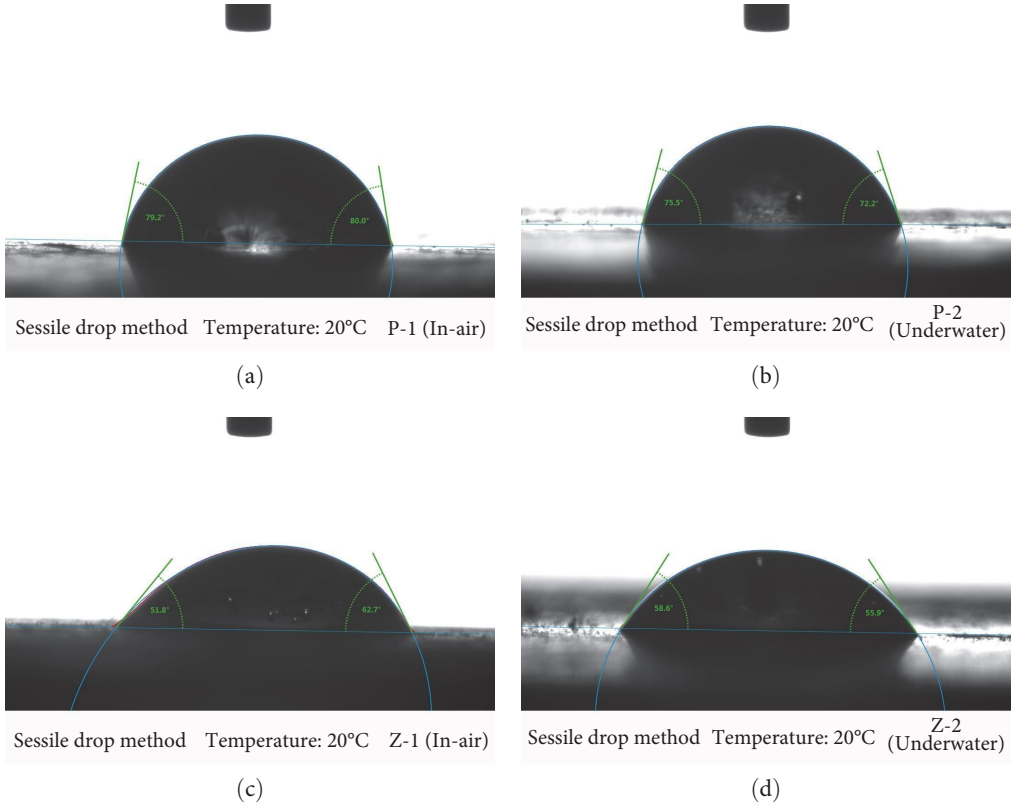

Figure 8: Test images of partial contact angles, (a) P-1 (in-air), (b) P-2 (underwater), (c) Z-1 (in-air), and (d) Z-2 (underwater).

significant change in the contact angle size for Z-type specimens. This indicates that it had a more stable hydrophobic property. When tested with the nonpolar liquids (diiodomethane), both the P-type and Z-type specimens showed varying decrease degrees in the contact angle size. The reduction for P specimens was 5.65% and for Z specimens was 9.46%. According to the results, the Z-type specimens had a larger drop and thus had lower hydrophobic stability than the P-type specimens. However, it also demonstrated that the two different states of CH_3-NS were beneficial in increasing the material's hydrophobicity.

Based on the data from the contact angle test, the results of the calculation of the surface free energy are shown in Table 13.

The data analysis revealed that the polar force component magnitude (sum of hydrogen bonding forces and dipole moment forces) of the surface tension of the specimen was the main factor influencing the surface free energy of the P-type specimens. If the polar force component is smaller, the surface of the specimen would be drier. Consequently, the hydrophobic property of the specimen will be improved, and the surface free energy will be reduced, resulting in better reinforcement. At the same time, the surface free energy of P-type specimens was affected by CH_3-NS in different states. The uncalcined CH_3-NS had a stronger dispersion force component. This could increase the material's hydrophobicity and decrease the surface free energy. Different states of CH_3-NS and the property of the specimens were the main factors influencing the surface free energy of the Z-type specimens. The uncalcined CH_3-NS had a stronger dispersion force component, which improved reinforcement performance. Meanwhile, the thinness of the reinforcement surface affected the polar force component.

3.5. FTIR Analysis. In this paper, FTIR was used to analyze the effect of different functional groups on each group of reinforced specimens. The test results are shown in Figure 9(a)–9(d).

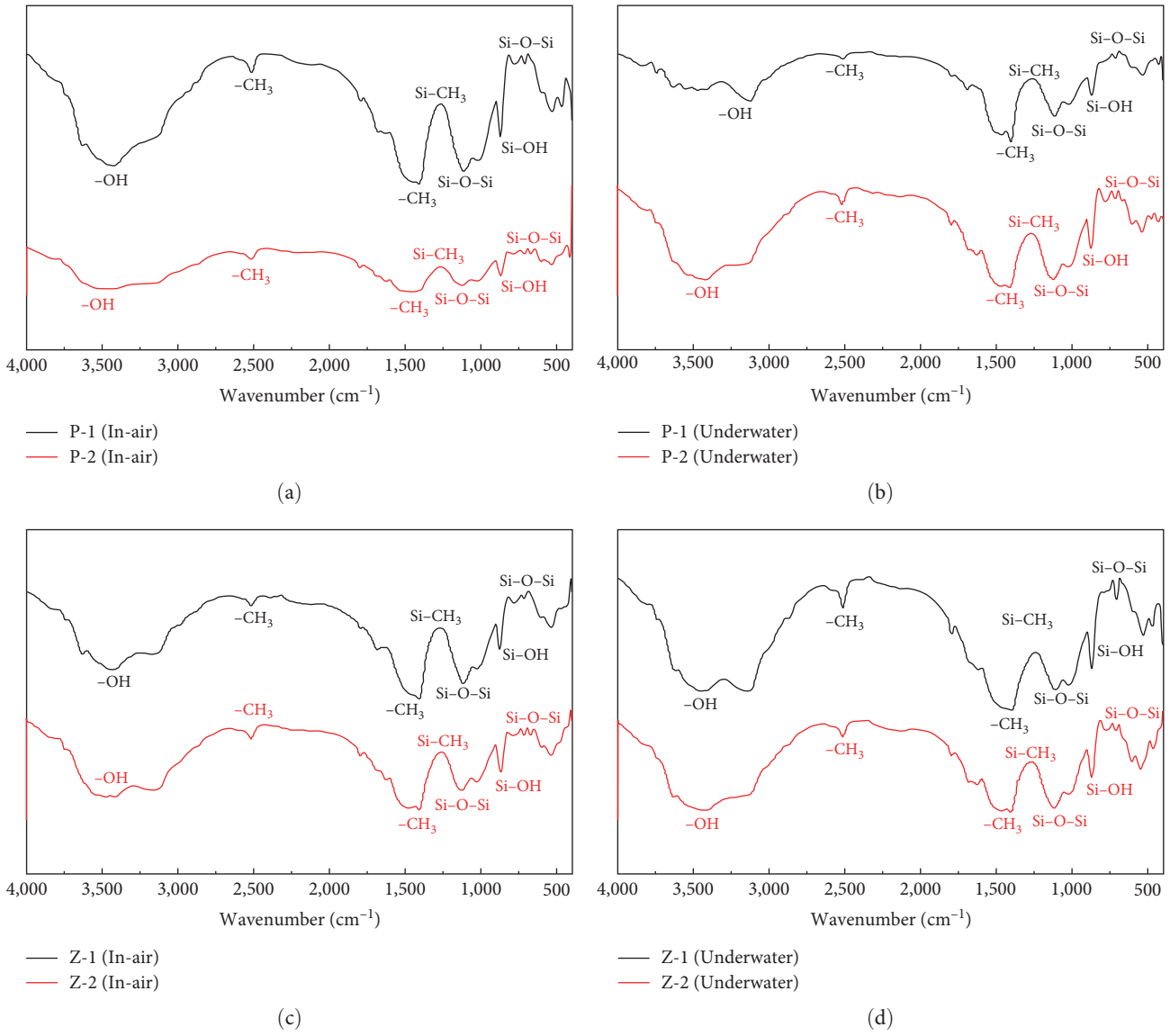

Figure 9: (a) FTIR analysis of P-type reinforcement concrete specimens under in-air conservation, (b) FTIR analysis of P-type reinforcement concrete specimens under underwater conservation, (c) FTIR analysis of Z-type reinforcement concrete specimens under in-air conservation, and (d) FTIR analysis of Z-type reinforcement concrete specimens under underwater conservation.

FTIR results demonstrated that under the in-air conservation, the hydrophobicity of P-type reinforcement concrete specimens was mainly provided by free $-CH_3$. The uncalcined CH_3-NS had more free $-CH_3$ and therefore exhibited better hydrophobic properties. For P-type reinforcement concrete specimens under underwater conservation, the infrared absorption peaks of free $-OH$ in the material appear at 3,124 cm^{-1} and 3,121 cm^{-1}, respectively. The free $-OH$ group is not evident in this type of specimen as seen from the peak, thus indicating that the group affecting the basic properties of the specimen is not the free $-OH$; The absorption peak near 871.8 cm^{-1} represents the stretching vibration of Si–OH, and the peak performance of this functional group on the spectrum shows a large change in trend. This is mainly due to the reaction of CH_3-NS with cement and water molecules, forming the functional group. Therefore, the main functional group that affects the reinforcement effect of the P-type reinforcement concrete specimens in the water environment is Si–OH.

For Z-type reinforcement concrete specimens under the in-air conservation, it can be seen from the Figure 9(c) that the peak performance of the main functional group Si–O–Si as a repair material is not obvious. The antisymmetric and symmetric stretching vibrations occur mainly at 692.4 and 1108.6 cm^{-1}. This indicates that the skeleton material of the Z-1,2 specimens under the in-air conservation was not significantly affected. The characteristic absorption peak of $Si–CH_3$ is more pronounced. This is mainly related to the free $-CH_3$ in CH_3-NS. The greater the number of free $-CH_3$, the more functional groups the material will combine in the overall reaction, which is beneficial to improve the hydrophobicity and reinforcement performance of the material.

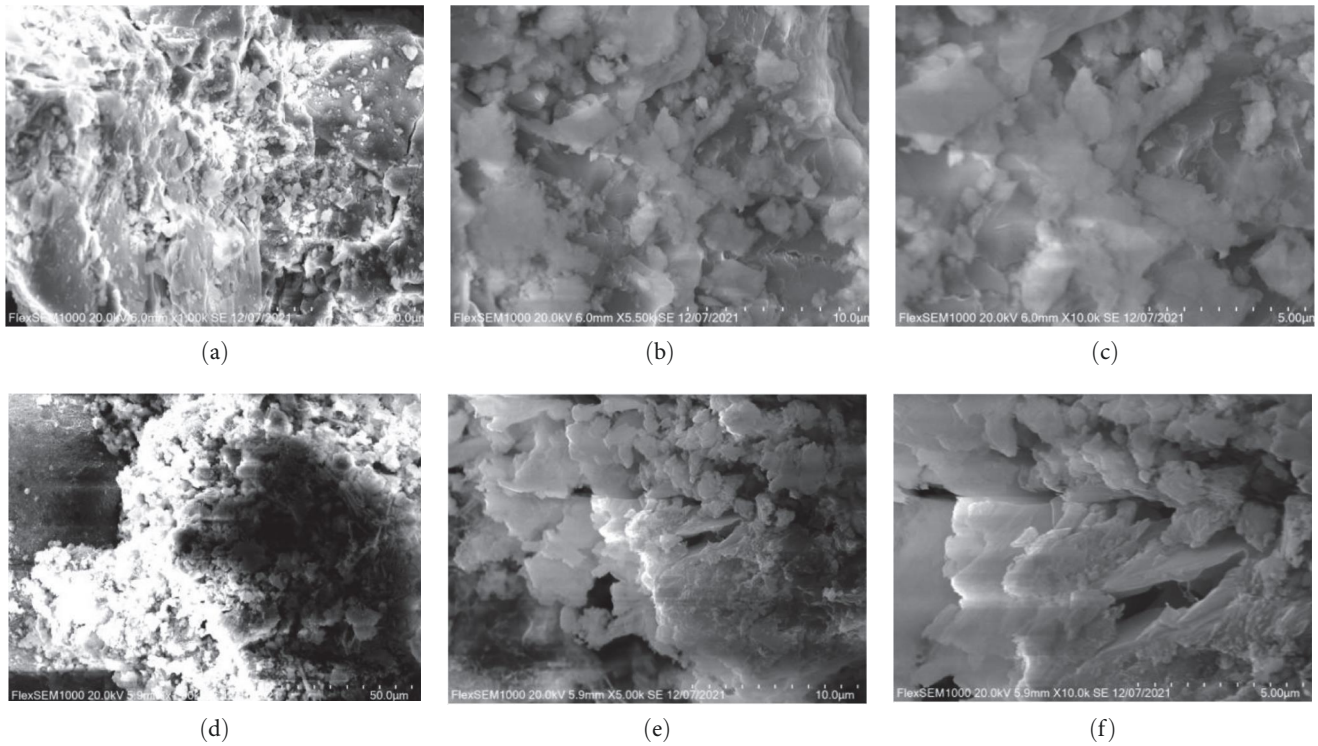

Figure 10: SEM images of P-type reinforcement concrete specimens under in-air conservation, (a) P-1 of 1 k times, (b) P-1 of 5 k times, (c) P-1 of 10 k times, (d) P-2 of 1 k times, (e) P-2 of 5 k times, and (f) P-2 of 10 k times.

For Z-type reinforcement concrete specimens under underwater conservation, the peaks around 2,514 and 1,396 cm^{-1} are the stretching and deformation vibrations of free $-CH_3$ in the specimen. The peak performance of Z-1 is even better, which is directly related to the fact that CH_3-NS has not been calcined. The peaks around 3,445 cm^{-1} represent the infrared absorption peaks of free −OH in the two materials, respectively. It's free −OH is not only provided by the material itself but also by the environmental factors. This leads to the fact that the peak performance of −OH is not obvious here, which leads to the fact that Si–OH is not considered the main functional group. The absorption peak near 871 cm^{-1} represents the stretching vibration of Si–OH. The peak performance of both of them is more consistent, which has some relation to the performance of free −OH. Compared with the specimen of the in-air conservation, the peak performance of Si–O–Si is more obvious. The antisymmetric and symmetric stretching vibrations occur mainly at 692.4 and 1,108.1 cm^{-1}. At the reinforcement interface, the presence of Si–O–Si provides additional assistance to the reinforcement during the underwater hardening process, resulting in better mechanical properties of the material. In summary, the different curing conditions and the different states of CH_3-NS do affect the hydrophobicity of the material and the reinforcement effect. Uncalcined CH_3-NS can provide more help for the reinforcement effect of the reinforcement material.

3.6. Microstructure Characteristics. Figures 10–13 illustrate the microstructure of the various types of specimens.

Based on the microstructure, the internal structure of P-type reinforcement concrete specimens was denser under the in-air conservation. The combination of CH_3-NS, high sulfur type ettringite of needle-shaped (AFt), and high-sulfur type ettringite of hexagonal flake (AFm), reduced the material's porosity. This also improved the later strength of the cement. Under underwater conservation, the microstructure of P-type reinforcement concrete specimens showed a different state. The porosity reduction of the P-1 specimen relied mainly on the AFm and AFt. The porosity reduction of the P-2 specimen relied mainly on the AFm. In addition, it possessed too little CH_3-NS and aluminum hydroxide gel of pompom shape (AH_3). Under the in-air conservation, the microstructure of Z-type reinforcement concrete specimens was significantly rougher. The AFt was perpendicular to the structure's surface, which reduced the porosity and increased the friction. C_2S produced an expansive AFt after the hydration reaction for Z-type reinforcement concrete specimens under the underwater conservation. This filled the voids of the hydration products and reduced the material's porosity.

4. Conclusions

This paper investigated the impact of CH_3-NS on UWC performance and assessed its reinforcement performance. The reinforcement mechanism was investigated by contact angle test, FTIR, and SEM. The principal results and the conclusions of this investigation are summarized as follows.

Adding CH_3-NS increased the fluidity of the UWC. The antiwashout resistance was reduced when too much CH_3-NS was added. The strength of concrete decreased slowly with increasing CH_3-NS admixture at 1%–3%. Comparing each

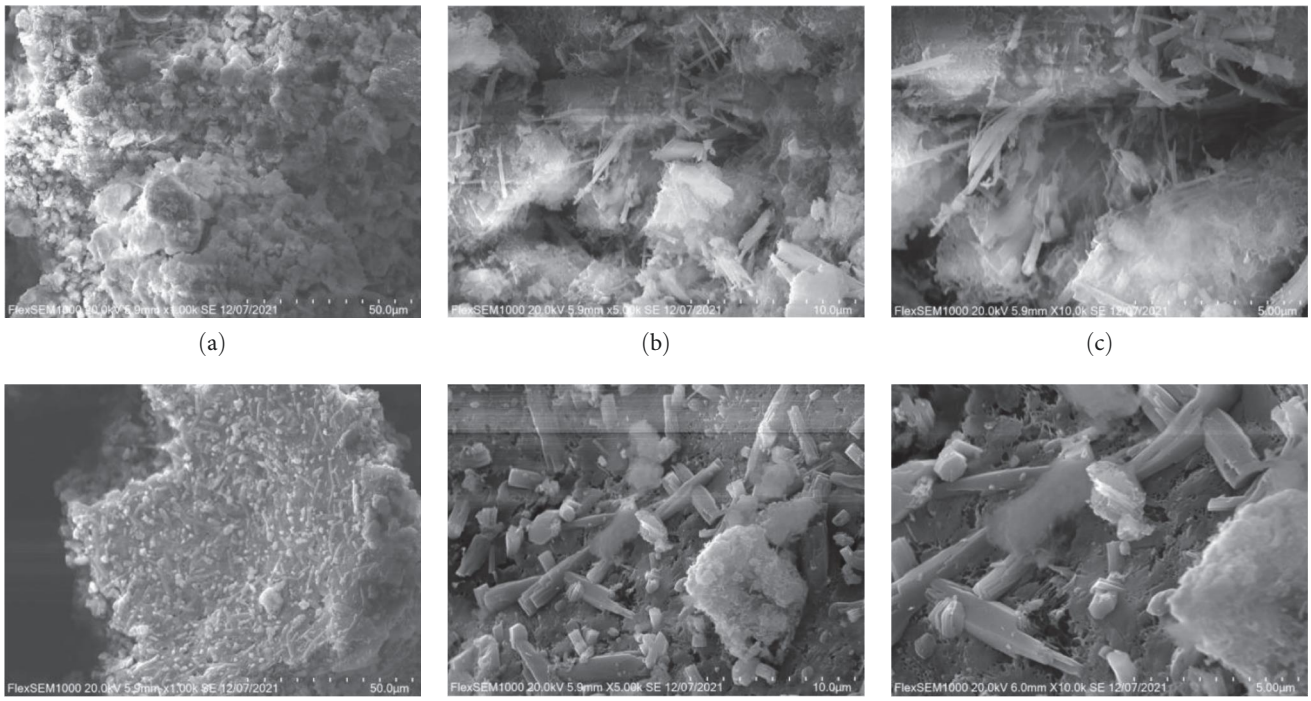

(a) (b) (c)

(d) (e) (f)

Figure 11: SEM images of P-type reinforcement concrete specimens under underwater conservation, (a) P-1 of 1 k times, (b) P-1 of 5 k times, (c) P-1 of 10 k times, (d) P-2 of 1 k times, (e) P-2 of 5 k times, and (f) P-2 of 10 k times.

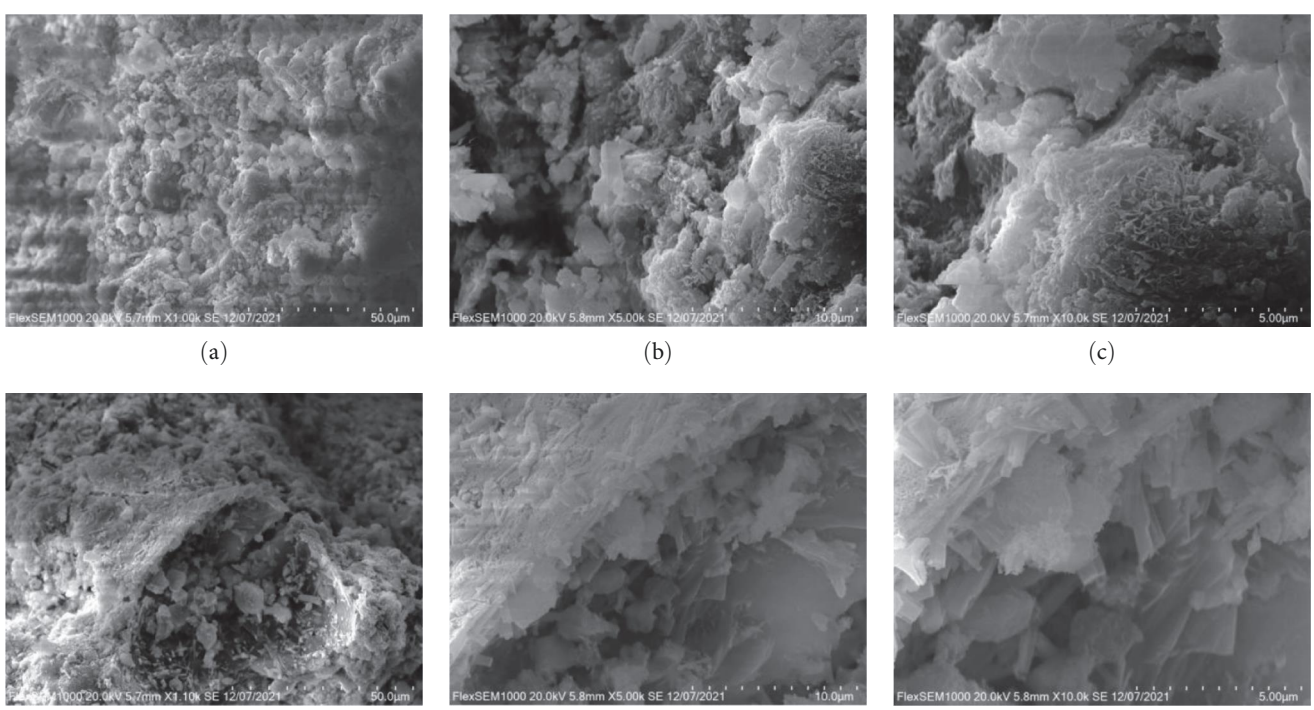

(a) (b) (c)

(d) (e) (f)

Figure 12: SEM images of Z-type reinforcement concrete specimens under in-air conservation, (a) Z-1 of 1 k times, (b) Z-1 of 5 k times, (c) Z-1 of 10 k times, (d) Z-2 of 1 k times, (e) Z-2 of 5 k times, and (f) Z-2 of 10 k times.

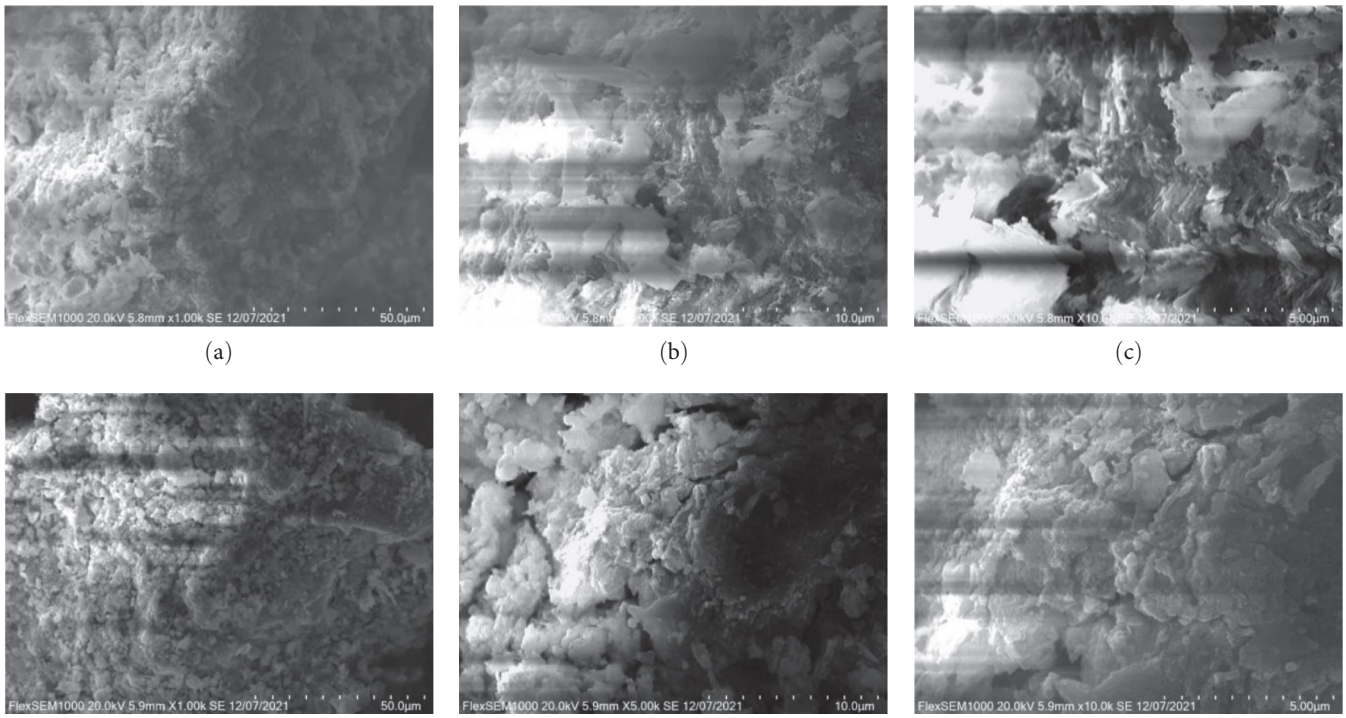

Figure 13: SEM images of Z-type reinforcement concrete specimens under underwater conservation, (a) Z-1 of 1 k times, (b) Z-1 of 5 k times, (c) Z-1 of 10 k times, (d) Z-2 of 1 k times, (e) Z-2 of 5 k times, and (f) Z-2 of 10 k times.

dose level revealed that UWC at 1% had the higherest strength.

Reinforcement tests showed that the addition of uncalcined CH_3-NS effectively enhanced the strength of P-type specimens after reinforcement. Meanwhile, it also shifted forward the peak and ultimate stresses of the specimens. The Z-type specimens still had the corresponding bearing capacity, so the addition of CH_3-NS in different states did not significantly help the strength at the early stage of reinforcement.

The main factor influencing the surface free energy of the P-type specimens was the polar force component magnitude of the surface tension of the specimens. The uncalcined CH_3-NS had a stronger dispersion force component. This could increase the material's hydrophobicity and decrease the surface free energy. The main factors influencing the surface free energy of the Z-type specimens were the different states of CH_3-NS and the properties of the specimen. In addition, the thinness of the reinforcement surface affected the polar force component.

The hydrophobicity of P-type reinforcement concrete specimens was mainly provided by free $-CH_3$ under in-air conservation. Si–OH was the main functional group affecting the P-type reinforcement concrete specimens under the underwater conservation. The hydrophobicity and reinforcement properties of Z-type reinforcement concrete specimens were mainly enhanced by Si–CH_3 under in-air conservation. Under the underwater conservation, the hydrophobicity and reinforcement properties of Z-type reinforcement concrete specimens were provided by free $-CH_3$, $-OH$, and Si–O–Si. Uncalcined CH_3-NS can provide more help for the reinforcement effect of the reinforcement material.

SEM analysis showed that incorporating uncalcined CH_3-NS resulted in a denser microstructure of the reinforcement material, improving its macro performance. In terms of microstructure, the reinforcement concrete specimens performed better under the in-air conservation, but the reinforcement concrete specimens also met all of the test requirements under the underwater conservation. Therefore, it is feasible to use CH_3-NS for underwater reinforcement.

Data Availability

The data used to support the findings of this study are included within the manuscript.

Conflicts of Interest

The authors declare that there are no conflicts of interest.

Acknowledgments

This research was supported by the National Natural Science Foundation of China (Grant No. 50708011), the Research Initiation Project of Xi'an Polytechnic University (Grant No. 310-107020368), and the State Scholarship Fund of China (Grant No. 202108610120). We thank Ms. Xi Qiao and Ms. Jin Yu for their help in the preparation of this manuscript.

References

[1] X. An, Q. Wu, F. Jin et al., "Rock-filled concrete, the new norm of SCC in hydraulic engineering in China," *Cement and Concrete Composites*, vol. 54, pp. 89–99, 2014.

[2] M. I. Balzannikov and A. A. Mikhasek, "The use of modified composite materials in building hydraulic engineering structures," *Procedia Engineering*, vol. 91, pp. 183–187, 2014.

[3] Z. L. Liang, C. M. Zhang, and J. W. Lei, "Application of non-dispersible underwater concrete in the three gorges hydroelectric power station," *Concrete*, vol. 12, pp. 78–80, 2006.

[4] C.-s. Jiang, L.-n. Lu, S.-b. Guan, Q.-j. Ding, and S.-g. Hu, "Preparation of high performance non-dispersible concrete," *Journal of Wuhan University of Technology-Mater. Sci. Ed*, vol. 19, no. 2, pp. 67–69, 2004.

[5] X. Li, F. Gui, and Q. Li, "Can hydropower still be considered a clean energy source? Compelling evidence from a middle-sized hydropower station in China," *Sustainability*, vol. 11, no. 16, p. 4261, 2019.

[6] W. Ren, L. H. Sneed, Y. Gai, and X. Kang, "Test results and nonlinear analysis of RC T-beams strengthened by bonded steel plates," *International Journal of Concrete Structures and Materials*, vol. 9, no. 2, pp. 133–143, 2015.

[7] A. Parghi and M. S. Alam, "Seismic behavior of deficient reinforced concrete bridge piers confined with FRP-a fractional factorial analysis," *Engineering Structures*, vol. 126, pp. 531–546, 2016.

[8] J. Ai and L. Shi, "Discussion of design and construction method on extraneous prestressed strengthening technique for bridge," *Dongnan Daxue Xuebao/Journal of Southeast University (Natural Science Edition)*, vol. 32, no. 5, pp. 771–774, 2002.

[9] D. E. Lehman, S. E. Gookin, A. M. Nacamuli, and J. P. Moehle, "Repair of earthquake-damaged bridge columns," *Structural Journal*, vol. 98, no. 2, pp. 233–242, 2001.

[10] H. Z. Saeed, Q. Z. Khan, A. Ahmed, S. M. Ali, and M. Iqbal, "Experimental and finite element investigation of strengthened LSC bridge piers under quasi-static cyclic load test," *Composite Structures*, vol. 131, pp. 556–564, 2015.

[11] J.-h. Zhu, M.-n. Su, J.-y. Huang, T. Ueda, and F. Xing, "The ICCP-SS technique for retrofitting reinforced concrete compressive members subjected to corrosion," *Construction and Building Materials*, vol. 167, pp. 669–679, 2018.

[12] Y. Wei, G. Wu, and Z. Wu, "Several innovative strengthening technologies for underwater piers," *Building Structure*, vol. 40, no. S1, pp. 683–686, 2010.

[13] N. H. Yi, J. W. Nam, S. B. Kim, and J.-H. J. Kim, "Evaluation of material and structural performances of developed aqua-advanced-FRP for retrofitting of underwater concrete structural members," *Construction and Building Materials*, vol. 24, no. 4, pp. 566–576, 2010.

[14] F. Menkulasi, H. Baghi, and D. Hall, "Rehabilitation of deteriorated timber piles with fiber reinforced polymer composites," *IABSE symposium report. International Association for Bridge and Structural Engineering*, vol. 109, no. 65, pp. 381–388, 2017.

[15] C. Zhang, X. Han, W. Zhou et al., "New progress of non-dispersible underwater concrete technology," *Concrete*, vol. 02, pp. 7–9, 2004.

[16] L. Courard, T. Piotrowski, and A. Garbacz, "Near-to-surface properties affecting bond strength in concrete repair," *Cement and Concrete Composites*, vol. 46, pp. 73–80, 2014.

[17] H. Wu, Z. Diao, and K. Fan, "Study on durability of non-dispersible concrete in seawater environment," *International Journal of Structural Integrity*, vol. 11, no. 3, pp. 443–452, 2020.

[18] M. Ali Sikandar, N. R. Wazir, A. Khan, H. Nasir, W. Ahmad, and M. Alam, "Effect of various anti-washout admixtures on the properties of non-dispersible underwater concrete," *Construction and Building Materials*, vol. 245, p. 118469, 2020.

[19] Y. Wang, L. Gu, and L. Zhao, "Beneficial influence of nanoparticles on the strengths and microstructural properties of non-dispersible underwater concrete," *KSCE Journal of Civil Engineering*, vol. 25, no. 11, pp. 4274–4284, 2021.

[20] F. Liu, B. Wang, M. Wang, and X. Yuan, "Analysis on pore structure of non-dispersible underwater concrete in saline soil area," *Journal of Renewable Materials*, vol. 9, no. 4, pp. 723–742, 2021.

[21] I. K. Jeon, B. H. Woo, D. H. Yoo, J. S. Ryou, and H. G. Kim, "Evaluation of the hydration characteristics and anti-washout resistance of non-dispersible underwater concrete with nano-SiO_2 and MgO," *Materials*, vol. 14, no. 6, p. 1328, 2021.

[22] J. Yang and J. R. Chen, "Surface free energies and steam stability of methyl-modified silica membranes," *Journal of Porous Materials*, vol. 16, no. 6, pp. 737–744, 2009.

[23] J. Yang, W. Fan, H. Hou, Y. Guo, D. Jia, and X. Xing, "Effect of DMF addition on the phase-chemical structure of Pd-doped methyl-modified silica membrane materials calcined in air atmosphere," *Ferroelectrics*, vol. 528, no. 1, pp. 83–89, 2018.

[24] O. Sengul and M. A. Tasdemir, "Compressive strength and rapid chloride permeability of concretes with ground fly ash and slag," *Journal of Materials in Civil Engineering*, vol. 21, no. 9, pp. 494–501, 2009.

[25] W. Chalee and C. Jaturapitakkul, "Effects of W/B ratios and fly ash finenesses on chloride diffusion coefficient of concrete in marine environment," *Materials and Structures*, vol. 42, no. 4, pp. 505–514, 2009.

[26] M. Harilal, V. R. Rathish, B. Anandkumar et al., "High performance green concrete (HPGC) with improved strength and chloride ion penetration resistance by synergistic action of fly ash, nanoparticles and corrosion inhibitor," *Construction and Building Materials*, vol. 198, pp. 299–312, 2019.

[27] Y. Q. Zhang and Y. Dong, "Effect of fly ash and silica fume on the performance of underwater self-compacting concrete," *Concrete*, vol. 10, pp. 133–137, 2021.

[28] M. Zhang, F.-m. Wang, K. Ye, Z.-g. Wu, and Y. Zeng, "Effect of fly ash and slag on anti-washout underwater concrete," *Bulletin of the Chinese Ceramic Society*, vol. 35, no. 8, pp. 2611–2616, 2016.

[29] J. Yang, Y. L. Wang, B. S. Li, and Y. Li, "Calculation and comparison on the surface free energy of methyl-modified silica films," *Materials Reports*, vol. 27, no. 22, pp. 134–137 146, 2013.

[30] China National Petroleum Corporation, *China National Petroleum Corporation Enterprise Standard: Technical Specification for Underwater Non-dispersed Concrete Construction Q/CNPC 92-2003*, China National Petroleum Corporation., 2003.

[31] China Electric Power Press, *The People's Republic of China Electric Power Industry Standard: Test Code on Antiwashout Underwater Concrete DL/T 5117-2021*, China Electric Power Press, 2021.